CHAPTER-2

SPICE-Based Compact Model for Voltage-Induced Magnetocapacitance in Magnetic Tunnel Junctions

The part of the work is adopted from-

J. Rajpoot, R. Paul, and S. Verma, "SPICE-Based Compact Model for Voltage-Induced Magnetocapacitance in Magnetic Tunnel Junctions," ***IEEE Transactions on Magnetics***, vol. 59, no. 9, pp. 1-8, Sept. 2023, Art no. 7200108, **doi: 10.1109/TMAG.2023.3296830**.

Abstract:

Ensuring faster data processing and higher integration density while meeting the power budget is a challenging task as the world is moving towards next-generation computing. Therefore, researchers are looking for innovative ways to make computation more efficient. Magnetic tunnel junction (MTJ) devices have received enormous attention in recent years due to their non-volatility, low power consumption, high tunneling magnetoresistance (TMR), and scalability. However, TMR degradation with bias voltage became a significant deficiency of the MTJ device. Another prominent phenomenon, *i.e*., tunnel magnetocapacitance (TMC), has been observed in the MTJ, which has high magnetic sensitivity, high thermal stability, and robustness to the applied bias voltage. Several MTJ models have been introduced in the past to emulate the magnetic switching behaviour in MTJs, but they do not incorporate the TMC effect. This work presents a SPICE-compatible STT-MTJ model, which incorporates both TMR and TMC effects. Here, the voltage-induced TMC effect is modeled using a combination of the Debye-Fröhlich (DF) model using a Zhang-sigmoid theory along with the parabolic barrier approximation (PBA) and spin-dependent drift-diffusion (SDD) model, which perfectly emulates the magnetocapacitance behaviour with respect to bias voltage and frequency. Furthermore, the proposed compact model is validated using HSPICE simulations and demonstrates good agreement with experimental data. This model can be used to implement new spintronics applications such as non-volatile logic-in-memory, spin logic devices, highly sensitive magnetic sensors, designing read-out circuits for sensors, and neuromorphic computing.

2.1 Introduction:

Spintronics is one of the promising fields for next-generation electronic devices that can enable low-power operation while retaining computation capability. Magnetic tunnel junction (MTJ) is a spintronics device that has garnered considerable attention in recent years because of its appealing characteristics, such as nonvolatility, faster data processing, higher integration density, and low power consumption. This device comprises two ferromagnetic layers separated by a thin insulating layer, which results in a significant tunnel magnetoresistance (TMR) effect [50]. Logic-in-memory (LiM) [174], spin-based logic, data read heads in HDDs, magnetic sensors [175], magnetoresistive random-access memory (MRAM) [176], and neuromorphic computing are typical examples of practical applications that rely on this TMR effect in MTJ device.

The major design challenge when using MTJs is the robustness of TMR with biasing voltage since TMR decreases significantly with the bias voltage. This has made researchers and designers to switch their attention toward its analogous effect, *i.e.*, tunnel magnetocapacitance (TMC) [69]. TMC is observed to have high magnetic sensitivity, frequency-dependence, thermal stability, and robustness against bias voltage (increase with biasing voltage) [71]. Furthermore, the $V_{1/2}$ factor (applied voltage at which the TMR or TMC becomes half of the unbiased value) of TMC in MTJ is reported to be twice as high as that of TMR [75]. Thus, the research in TMC and a compact model that captures the inherent physics is quite important for exploring new applications using MTJ devices. The capacitance of MTJ is high for parallel (P) configuration and low for anti-parallel (AP) configuration due to the TMC effect. Furthermore, it has been observed that the TMC effect is highest at a specific

frequency and increases with bias application. Magnetocapacitance is induced in CoFeB/MgO/CoFeB-based MTJs due to the accumulation of charges between the ferromagnetic and insulator layers. Due to high conductance in the P configuration, a substantial amount of charge builds up at the interface of the ferromagnetic and insulator layers, whereas a small amount of charge builds up in the AP configuration. The voltage and frequency dependence of the TMC effect can be explained by the Debye-Fröhlich model (DF) [71] using the Zhang-sigmoid theory [58], parabolic barrier approximation (PBA), and spin-dependent drift-diffusion (SDD) model [76].

Previously, several compact models have been proposed to emulate STT-MTJs that are compatible with SPICE [95], [120], [121], [177]. In [121], the researcher presented a compact model for perpendicular-plane MTJ (PMTJ), describing the tunnel magnetoresistance, switching behaviour, and a physical model for static, dynamic, and stochastic effects. A model proposed in [95] incorporates STT and external magnetic field to capture the magnetization dynamics, thermal variation, and self-heating. In [120], an adaptive compact MTJ model with asymmetry effects is proposed, where STT and voltage-controlled magnetic anisotropy (VCMA) switching mechanisms are utilized to control dynamic behaviour. The work in [177] presents a compact model with spin-polarization asymmetry of PMTJ to capture the spin transfer asymmetry on the fast-switching process. All these models lack the TMC effect. This work introduces a SPICE-compatible STT-MTJ model that uses a combination of the DF model based on the Zhang-sigmoid theory along with the PBA and SDD model to capture the dependence of magnetocapacitance on the frequency with and without bias voltage for both P and AP configurations and the TMC effect.

2.2 Compact Model of MTJ with Magnetocapacitance

2.2.1. MTJ Device Structure

The MTJ has a multilayered structure consisting of both ferromagnetic and non-magnetic materials. **Figure 2.1** displays a three-layer structure with a tunnel barrier (TB) layer located between the free layer (FL) and the pinned layer (PL). The PL is composed of CoFeB and has a fixed magnetization. The TB employs MgO as a dielectric and has a few nanometers of thickness [178]. The FL serves as the data-storage layer, and its magnetization direction can be controlled via spin-polarized current. The TMR effect occurs when the relative magnetization of the ferromagnetic layers alters their alignment, causing a change in the tunneling current in the MTJ. When the magnetization in the FL is P (AP) to the PL, the MTJ's resistance becomes low (high) due to the TMR effect. Here, only STT and field-assisted STT techniques are used to flip the magnetization of the FL.

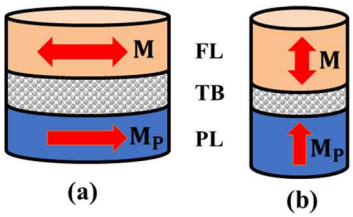

Figure 2.1 MTJ structures (a) In-plane MTJ (iMTJ) (b) Perpendicular-plane MTJ (pMTJ)

2.2.2. Magnetic Anisotropy Module

The direction of magnetization in magnetic materials is determined by magnetic anisotropy, which provides an easy axis along which the magnetization can easily be aligned. The classification of magnetic anisotropy is based on the alignment of the easy axis and sources of magnetic anisotropy, resulting in two common types: in-plane magnetic anisotropy (IMA) and perpendicular-plane magnetic anisotropy (PMA). In the case of IMA, the easy axis of the magnetic material is parallel to its plane. On the other hand, PMA tries to align the

magnetization perpendicular to the plane of the magnetic material. PMA can be further classified based on its origin: crystalline PMA and interfacial PMA [96]. The demagnetization field is also given as

$$H_d = \frac{2K_{eff}}{M_S} \tag{2.1}$$

where, K_{eff} is the effective magnetic anisotropy energy density of the material, also defined as follows

$$K_{eff} = K_{\parallel} + K_{\perp} \tag{2.2}$$

where,

$$K_{\parallel} = 2\pi(N_{dy} - N_{dx})M_s^2 \tag{2.3}$$

$$K_{\perp} = K_b + \frac{K_i}{t_{FL}} - 2\pi N_{dz} M_s^2 \tag{2.4}$$

where, M_S represents the saturation magnetization, N_d = [N_{dx}, N_{dy}, N_{dz}] is the shape-dependent demagnetization coefficient, K_i for interfacial anisotropy density, and $K_b$is the bulk anisotropy density. In an elliptical-shaped in-plane MTJ (iMTJ), a substantially high demagnetization factor N_{dz} is required to retain the magnetization of the FL in the easy plane. When the FL thickness exceeds 2 nm, it exhibits a significantly lower interfacial anisotropy density (K_i/t_{FL}) compared to the demagnetization density factor ($2\pi N_{dz} M_s^2$), leading to a negative perpendicular anisotropy ($K_{\perp}$). The interface PMA occurs when the thickness of the FL (t_{FL}) is less than the critical thickness (t_c) *i.e.,* $t_{FL} < t_c$, at the interface with a tunnel barrier (TB). In the cylindrical pMTJ device, the in-plane anisotropy ($K_{\parallel}$) becomes zero due to the equal values of the demagnetization factors N_{dx} *and* N_{dy}. However, the interfacial anisotropy density (K_i/t_{FL}) increases much higher than the demagnetizing factor, resulting in an exceptionally high $K_{\perp}$ [96].

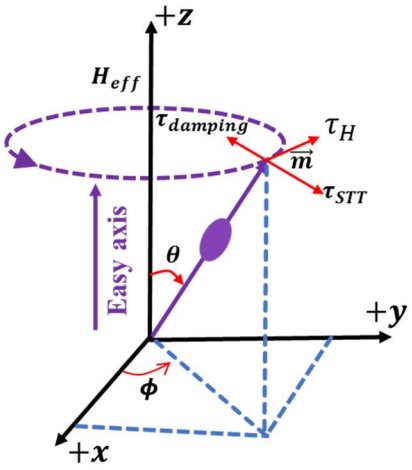

Figure 2.2 Illustration of magnetization components of the free layer

2.2.3. Magnetization Dynamics Module

Vector representation of magnetization of the FL $\vec{M} = [M_x, M_y, M_z]$ as shown in **Figure 2.2** and the magnetization of the PL $\vec{M}_P$= $[M_{Px}, M_{Py}, M_{Pz}]$ can be written as

$$\vec{M} = sin\theta cos\phi a_x + sin\theta sin\phi a_y + cos\theta a_z \quad 2.5$$

$$\vec{M}_P = sin\theta_h cos\phi_h a_x + sin\theta_h sin\phi_h a_y + cos\theta_h a_z \quad 2.6$$

The magnetization dynamics of FL ($\vec{M}$) under the influence of an effective magnetic field (H_{eff}**)** can be represented using the Landau-Lifshitz-Gilbert-Slonczewski (LLGS) equation [178] as

$$\frac{d\vec{M}}{dt} = \alpha\left(\vec{M} \times \frac{d\vec{M}}{dt}\right) - \gamma\vec{M} \times (\vec{M} \times H_{eff}) \quad 2.7$$

where, α and γ are the Gilberts damping constant and gyromagnetic ratio, respectively. Here H_{eff} is the vector sum of the crystalline anisotropy field (H_k), demagnetization field (H_d), thermal field (H_{th}), spin-torque field (H_S), and external magnetic field (H_{ext}) can be expressed as

$$H_{eff} = H_k + H_d + H_{th} + H_S + H_{ext} \quad 2.8$$

The crystalline anisotropy field (H_k) coincide with the easy axis. The demagnetization field (H_d) can be represented as in-plane ($H_{dx}\ and\ H_{dy}$) and perpendicular plane (H_{dz}) components

$$H_{dxy} = 4\pi\left(N_{dy} - N_{dx}\right)M_S \tag{2.9}$$

$$H_{dz} = 4\pi N_{dz} M_S \tag{2.10}$$

Here, the thermal noise field is presented as an external magnetic field component (H_{th}). The spin-torque equivalent magnetic field (H_S) created by current density (J) has two components: $H_{STT}\ and\ H_{FLT}$**,** the magnetic fields associated with STT and field-like torque (FLT) [179], respectively.

$$H_S = H_{STT} + H_{FLT} \tag{2.11}$$

The H_{STT} can be modeled as

$$H_{STT} = \frac{\hbar \eta_{STT} J}{2qM_S V H_k}\left(\vec{M} \times \vec{M}_P\right) \tag{2.12}$$

where, $\hbar$ is the reduced plank's constant, q is the electron charge, and V is the volume of an MTJ's FL. Herein, η_{STT} is the spin polarization efficiency, which depends on the spin polarization factor (P) and can be expressed as

$$\eta_{STT} = \frac{P}{2\left(1+P^2(\vec{M}\ .\ \vec{M}_P)\right)} \tag{2.13}$$

In an IMTJ device, the magnitude of a H_{FLT} can be as high as 30-40 % of the STT [179], but it is insignificant in a PMTJ device [179], [180]. The H_{FLT} can be specified as

$$H_{FLT} = \frac{\hbar \eta_{FLT} J}{2qM_S V H_k}\vec{M}_P \tag{2.14}$$

The spin polarization efficiency η_{FLT} can be modeled as

$$\eta_{FLT} = f_P \eta_{STT} \tag{2.15}$$

where, f_p is denoted as the pre-factor, which can be in the range of 0.1-0.4 for an IMTJ device. Alternatively, the LLGS equation can also be expressed as

$$\frac{1+\alpha^2}{\gamma H_k}\begin{bmatrix}\frac{d\theta}{dt}\\ \frac{d\phi}{dt}\end{bmatrix} = \tau_u + \tau_d + \tau_{th} + \tau_{STT} + \tau_{FLT} \tag{2.16}$$

Here τ is the torque associated with the relevant magnetic field as defined in equations (2.8) to (2.11). Further, for a PMTJ device, the time derivative components of respective magnetic fields can be expressed as

$$\tau_u = -\begin{bmatrix}\alpha sin\theta cos\theta\\ cos\theta\end{bmatrix} \tag{2.17}$$

$$\tau_d = -h_{ep}\begin{bmatrix}sin\theta cos\phi(sin\phi + \alpha cos\theta cos\phi)\\ cos\phi(cos\theta cos\phi - \alpha sin\phi)\end{bmatrix} \tag{2.18}$$

$$\tau_{th} = h_{th}\begin{bmatrix}(sin\phi + \alpha cos\theta cos\phi)H_x\\ +(\alpha cos\theta sin\phi - cos\phi)H_y - \alpha sin\theta H_z)\\ \frac{1}{sin\theta}(cos\theta cos\phi - \alpha sin\phi)H_x\\ +\frac{1}{sin\theta}(cos\theta sin\phi + \alpha cos\phi)H_y - H_z\end{bmatrix} \tag{2.19}$$

$$\tau_{STT} = h_{STT}\begin{bmatrix}(cos\theta cos\phi - \alpha sin\phi)H_{sx}\\ +(cos\theta sin\phi + \alpha cos\phi)H_{sy} - sin\theta H_{sz}\\ \frac{1}{sin\theta}(-\alpha cos\theta cos\phi - sin\theta)H_{sx}\\ +\frac{1}{sin\theta}(cos\phi - \alpha cos\theta sin\phi)H_{sy} + \alpha H_{sz}\end{bmatrix} \tag{2.20}$$

$$\tau_{FLT} = h_{FLT}\begin{bmatrix}(cos\theta cos\phi - \alpha sin\phi)H_{sx}\\ +(cos\theta sin\phi + \alpha cos\phi)H_{sy} - sin\theta H_{sz}\\ \frac{1}{sin\theta}(-\alpha cos\theta cos\phi - sin\theta)H_{sx}\\ +\frac{1}{sin\theta}(cos\phi - \alpha cos\theta sin\phi)H_{sy} + \alpha H_{sz}\end{bmatrix} \tag{2.21}$$

where, $h_{ep} = \frac{4\pi M_S}{H_k}$, $h_{th} = \frac{H_{th}}{H_k}$, $h_{STT} = \frac{\hbar \eta_{STT} J}{2qM_S V H_k}$, $h_{FLT} = \frac{\hbar \eta_{FLT} J}{2qM_S V H_k}$

2.2.4. MTJ Resistance Module

The magnetoresistance is associated with the spin orientation of the ferromagnetic layer between the two terminals of the MTJ device. This magnetoresistance is modeled and incorporated inside the MTJ model as a SPICE subcircuit. Herein, the TMR is determined by the spin polarization (P) and the bias voltage (V) across the MTJ and represented as

$$TMR(V,T) = \frac{2P(T)^2}{1-P(T)^2}\left\{\frac{1}{1+\left(V/V_0\right)^2}\right\} \quad 2.22$$

wherein, temperature-dependent spin polarization $P(T) = P_0(1 - \alpha_{sp}T^{3/2})$. Here P_0 represents the spin polarization at 0K, and T represents absolute temperature. α_{sp} is the material-dependent constant. Here, the resistance-area product (RA) of the device is used to determine the R_P of an MTJ. The parallel and anti-parallel resistance of an MTJ, *i.e.,* R_P and R_{AP} are determined using the following relationships.

$$R_P = RA/\left(\frac{\pi}{4} \times l_x \times l_y\right) \quad 2.23$$

$$R_{AP} = (1 + TMR(V,T))R_P \quad 2.24$$

$$R_{MTJ} = (1 + cos\theta) \times \frac{(R_P - R_{AP})}{2} + R_{AP} \quad 2.25$$

where, V_0 is the fitting parameter. Once the RA value is determined, R_P and R_{AP} are computed by considering the MTJ area and TMR in the proposed model.

2.2.5. Thermal Noise Module

The stochastic thermal noise, which depends on the temperature, can affect the magnetization dynamics of the MTJ. Using a random field, the stochastic nature of magnetization switching is included in the proposed model, which helps to accurately capture the effect of thermal noise during MTJ switching. Thermal noise has been implemented in this model using a resistor in parallel with a thermal noise current source, resulting in the computation

of a random thermal field $H_{th}(x, y, z)$ [181], as shown in **Figure 2.3**.

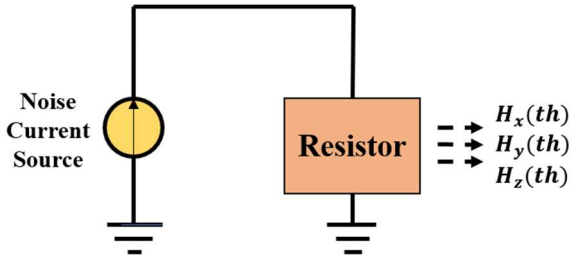

Figure 2.3 Thermal noise equivalent circuit diagram

This random thermal field is added to the LLGS equation, which implements the stochastic thermal fluctuations induced in MTJ, resulting in a stochastic LLGS equation. The magnitude of the random thermal field is given by

$$H_{th} = \sqrt{\frac{\alpha}{1+\alpha^2}\frac{2k_B T}{\gamma\mu_0 Ms(T) V\delta(t)}} \tag{2.26}$$

where, $\delta(t)$ represents the simulation time step, k_B represents Boltzmann's constant, α represents the damping ratio, and γ represents the gyromagnetic ratio. The effect of saturation magnetization is also considered using $M_S(T) = M_{S0}(1 - T/T_C)^{\beta}$. Here, M_{S0} represents the saturation magnetization at 0K, T is absolute temperature, T_C is Curie's temperature, and β represents the material-dependent constant. The influence of stochastic thermal variations on MTJ switching is taken into consideration by the SPICE model, and a similar approach has been used in the earlier model [181].

2.2.6. MTJ Capacitance Module

The frequency and bias voltage dependence of magnetocapacitance for P, as well as AP configuration, is calculated using a combination of the DF model and the Zhang-sigmoid theory along with the conventional PBA [76] given by

$$C_{P(AP)}^{DF-Z} \quad (f,V) = \frac{1}{1-e(1-\kappa)V/4\phi_0} \times \left[C_{\infty,P(AP)} + \frac{C_{0,P(AP)} - C_{\infty,P(AP)}}{2} \times \left(1 - \frac{sinh[\beta_{P(AP)} ln(2\pi f \tau_{P(AP),V})]}{cosh[\beta_{P(AP)} ln(2\pi f \tau_{P(AP),V})] + cos(\beta_{P(AP)} \pi/2)}\right)\right] \quad 2.27$$

Furthermore, from Jullière's model, the relation between the relaxation time of electrons in P and AP states, *i.e.*, τ_P and τ_{AP} is given by

$$\tau_{AP} = \frac{1+P^2}{1-P^2}\tau_P \quad 2.28$$

where, P is the spin polarization of the FM layers. The SDD model suggests that the interface of the FM and insulator layer creates tiny screening charge dipoles as a result of the accumulation of minority spins and depletion of majority spins in the AP configuration. This creates an additional serial capacitance during AP configuration, expressed as

$$C_{AP}^{SDD}(V) = eS\frac{n_{0,AP}\lambda}{\kappa V} \quad 2.29$$

Wherein, λ represents the characteristic screening length at the interface in the AP configuration, $n_{0,AP}$ is screening charge density, and S is the junction area of MTJ. Therefore, the effective capacitance $C_{AP}(f,V)$ under the applied bias voltage (V) in the AP configuration [76] is given by

$$C_{AP}(f,V) = \left(\frac{1}{C_{AP}^{DF-ZSP}(f,V)} + \frac{1}{C_{AP}^{SSD}(V)}\right)^{-1} \quad 2.30$$

where, $C_{AP}^{DF-ZSP}(f,V)$ is the capacitance modeled by the DF-ZSP model, and $C_{AP}^{SSD}(V)$ represents capacitance modeled using the SDD model. TMC is expressed as

$$TMC\ ratio = \frac{C_P(f,V) - C_{AP}(f,V)}{C_{AP}(f,V)} \quad 2.31$$

$$C_{MTJ}(f,V) = (1 + cos\theta) \times \frac{(C_P(f,V) - C_{AP}(f,V))}{2} + C_{AP}(f,V) \quad 2.32$$

where, $C_{MTJ}(f,V)$ represents the magnetocapacitance, which is C_P and $C_{AP,}$ depending on

the angle (θ) between the magnetization direction of PL and FL of MTJ in the proposed model.

The proposed MTJ capacitance module, defined as a SPICE subcircuit incorporating the equations from (2.27) to (2.32), is first verified with respect to the experimental data in [76]. Herein, the parameters are taken accordingly from [76]. The junction area of MTJ is 1800 μm^2, $C_{\infty,P(AP)}$= 0.80 (0.90) nF $C_{0,P(AP)}$ = 1037 (1221) nF, $\beta_{P(AP)}$= 0.986 (0.999), τ_P= 0.0118 s and P_0 = 0.477. The frequency characteristics of magnetocapacitance and TMC under no bias for P and AP configurations are presented in **Figure 2.4**. Furthermore, the bias voltage dependence of magnetocapacitance and TMC at various frequencies are observed by performing DC analysis, as shown in **Figure 2.5**. The simulation results show good agreement with experimentally observed from [75], and [76].

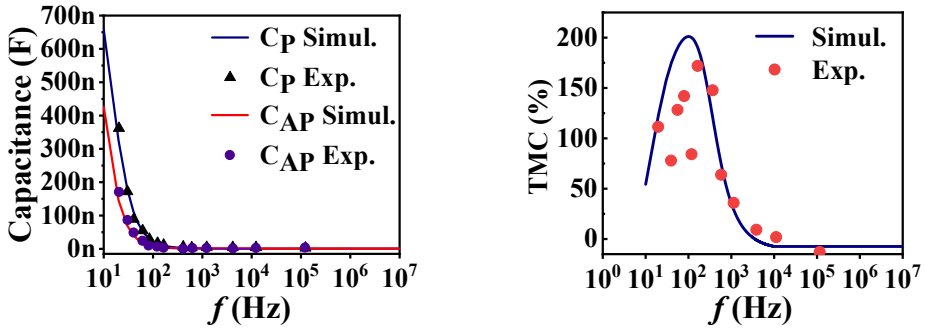

Figure 2.4 Frequency characteristics with experimental data under no bias of (a) magnetocapacitance and (b) tunnel magnetocapacitance

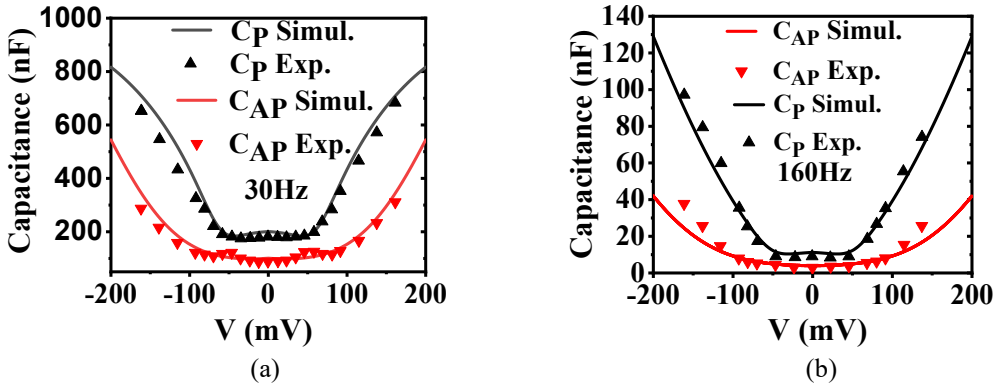

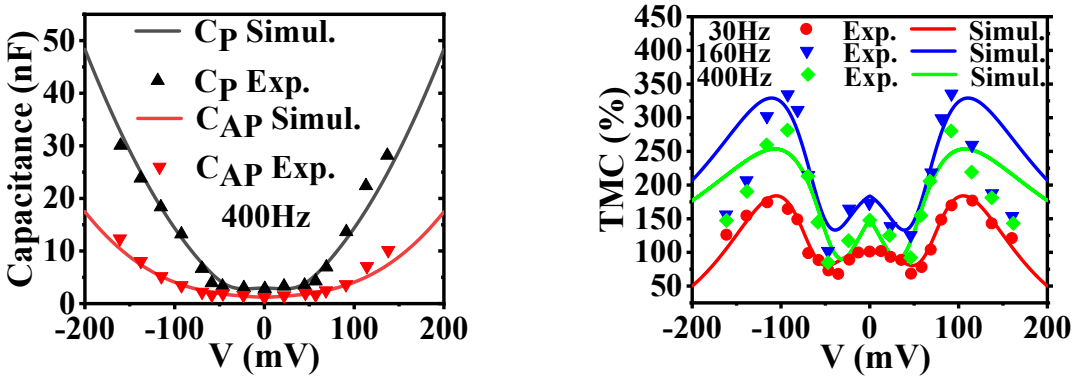

(c) (d)

Figure 2.5 Bias voltage dependence of magnetocapacitance and TMC for different frequencies, *i.e.,* (a) 30 Hz, (b) 160 Hz, (c) 400 Hz. (d) Variation of TMC (%) with a bias for all three frequencies using the junction area of MTJ is 1800 μm^2

2.3 SPICE Simulation Framework of MTJ Model

This work utilizes the existing HSPICE-compatible STT-MTJ models [95], [96], [120], [121], [172], [177], [178], [179], [180], [181], and further, to emulate the magnetocapacitance behaviour of MTJ, an additional capacitor module is integrated parallel to the resistor module as shown in **Figure 2.6(a)**. The model incorporates several subcircuits or modules, each demonstrating different aspects of MTJ physics, as shown in **Figure 2.6(b)**. These subcircuits include an LLG solver, heat diffusion, resistance module, capacitance module, and thermal noise. LLG subcircuit is used to emulate the MTJ switching behaviour using parameters such as magnetization (M_x, M_y, M_z), geometry (l_x, l_y, l_z), initial angle (θ_0), and initial polarization (P_0). It is done by employing the LLGS equation with STT and external magnetic field effects. To emulate the heating effect in MTJ. The heat diffusion module is employed, which utilizes an RC line model and incorporates two voltage sources to represent the initial temperature at each terminal of MTJ. The resistance module is used to calculate the TMR and resistance of MTJ, which is the function of magnetization, temperature, and

bias voltage. Similarly, the MTJ capacitance module is used to capture the capacitance of MTJ and TMC effect, which is modeled using the DF model and Zhang sigmoid model along with SDD and PBA approximation. This subcircuit depicts the dependence of capacitance on bias voltage, initial magnetization, and frequency of applied bias voltage.

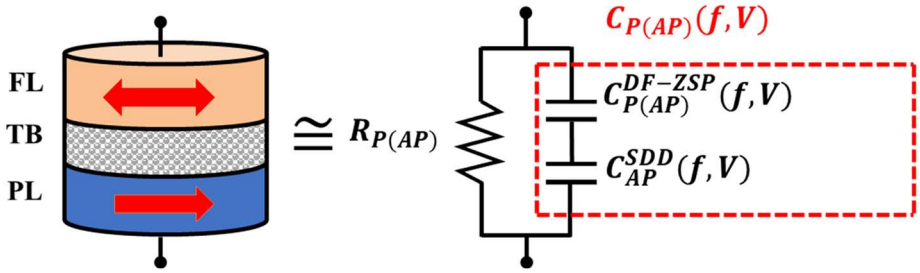

(a)

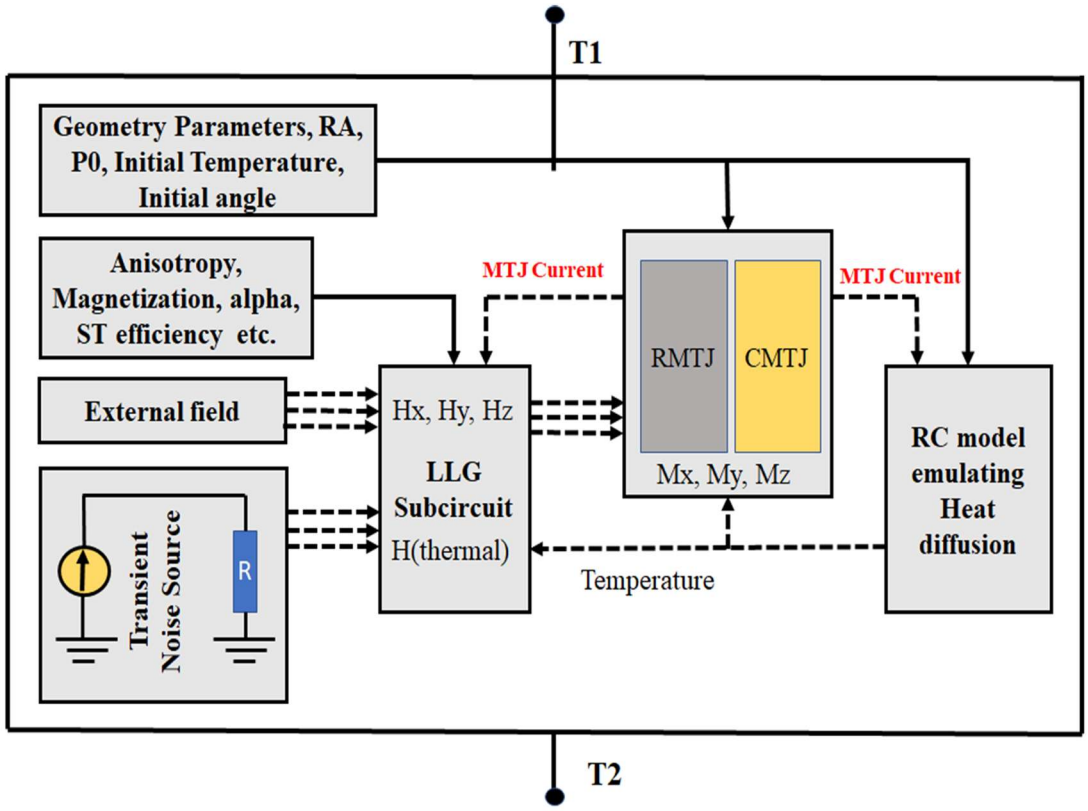

(b)

Figure 2.6 (a) Equivalent circuit model of MTJ (b) SPICE simulation framework for STT-MTJ model with magnetocapacitance.

Table 2.1 Key Parameters Utilized in the MTJ SPICE Model

List of User-Defined Model Parameters	
Description	**Value**
FL dimensions, $l_x \times l_y \times l_z$	32nm×96nm×2.44nm
Saturation Magnetization, M_{0s}	1210 emu/cm^3
Anisotropy Constant K_u	621600 erg/cm^3
Polarization Factor, P_0	0.477
Damping Factor, α	0.01
Temperature, TMP_0	300 K
Simulation Time Step, $\delta(t)$	1 ps
Uniaxial field strength, H_K	100 Oe
Resistance area product, RA	5 Ω μm^2
List of C_{MTJ} Subcircuit Parameter	
$C_{\infty,P(AP)}$	1.1(1.2) fF
$C_{0,P(AP)}$	1.4(1.6) pF
$\beta_{P(AP)}$	0.986(0.999)
τ_P	0.0118 s
γ	0.1

2.4 Simulation Results and Observation

To analyze and validate the proposed STT-MTJ framework and demonstrate its TMC capability, comprehensive HSPICE simulations are carried out using the parameters listed in **Table 2.1**. Further, a detailed parameter set used in the calculation of voltage-induced magnetocapacitance for different frequencies is given in **Table 2.2**. Herein, frequency characteristics, DC, and transient analyses are performed in order to compute the performance characteristics of MTJ under no bias and applied bias voltage for the circuit shown in **Figure 2.7**.

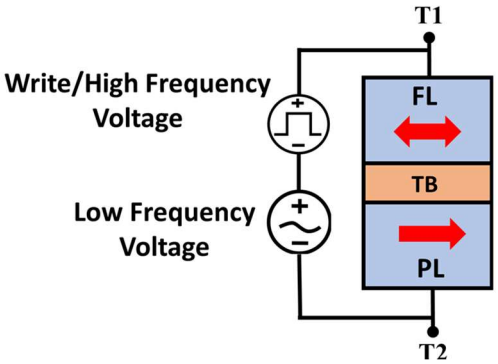

Figure 2.7 Simulation setup of IMTJ with the biasing condition to observe TMR and TMC effects.

Table 2.2 Frequency-Dependent Fitting Parameters Employed in Voltage-Induced TMC

f (Hz)	$\phi_{0,P(AP)}$ (eV)	$V_{0,P(AP)}$	$n_{0,P(AP)}$ (cm^{-3})	$K_{P(AP)}$ (V^{-1})	$\alpha_{P(AP)}$
30	0.168(0.0275)	0.059(0.108)	0.792	20(15)	80(15)
160	2.00(0.0460)	0.047(0.085)	0.354	22(18)	80(14)
400	0.841(0.0582)	0.036(0.053)	0.300	32(28)	92(10)

2.4.1. Frequency characteristics of TMC under no bias

The frequency characteristics of magnetocapacitance and TMC under no-bias conditions are demonstrated in **Figure 2.8(a)** and **2.8(b)**, respectively. It is observed that the value of C_P is greater than C_{AP}. Also, the value of $C_{P(AP)}$ decreases as frequency increases, with a peak of ~ 0.9 pF for P configuration and ~ 0.4 pF for AP configuration, and the value of the TMC is maximum (~300 %) at ~ 100 Hz. The variation of TMC with frequency at a bias voltage of 100 mV is also presented in **Figure 2.8(b)**.

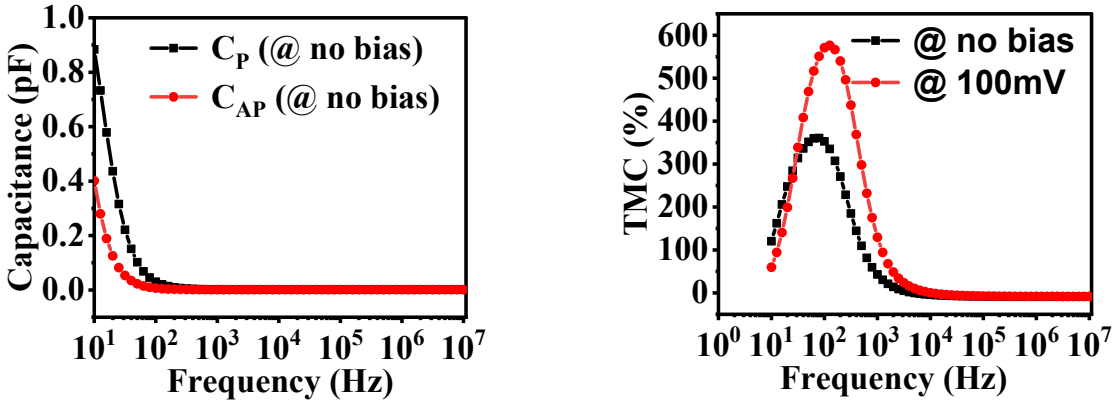

(a) (b)

Figure 2.8 Frequency characteristics of (a) magnetocapacitance and (b) TMC

2.4.2. DC analysis for voltage-induced TMC

To observe the voltage dependency of magnetocapacitance and TMC, the DC analysis is performed by applying a low-frequency sinusoidal voltage with a peak of 200 mV along with DC biasing. The simulation results, as depicted in **Figure 2.9**, illustrate the voltage

dependence of magnetocapacitance and TMC at various frequencies: **(a)** 30 Hz, **(b)** 160 Hz, and **(c)** 400 Hz. Furthermore, **Figure 2.9(d)** demonstrates the TMC variation with respect to a bias voltage, ranging from -200 mV to 200 mV. The observed magnetocapacitance and TMC results are consistent with previously calculated results [76], thereby validating the voltage-induced TMC effect using a combination of the DF model, Zhang-sigmoid theory, PBA, and SDD.

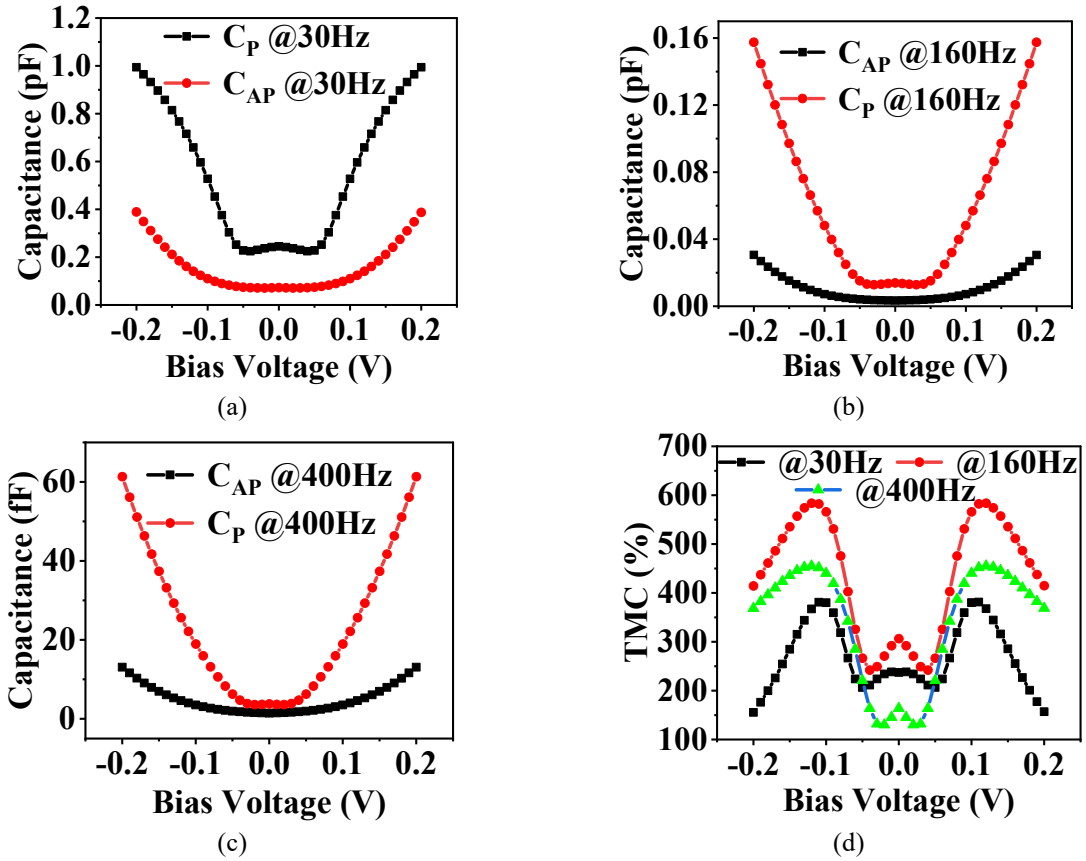

Figure 2.9 Voltage dependence of magnetocapacitance at various frequencies (a) 30 Hz, (b) 160 Hz, (c) 400 Hz. and (d) Depict the variation of TMC (%) with a bias voltage for various frequencies.

2.4.3. Transient analysis of MTJ

In order to investigate the behaviour of magnetoresistance and magnetocapacitance under dynamic conditions, the transient analysis is conducted by using the STT switching

mechanism with and without the assistance of an external magnetic field to switch the magnetization of the MTJ. STT switching is stochastic in nature, due to which the incubation delay is not always constant. Therefore, we apply a bias voltage of -1.2 V along with an external magnetic field of 0 Oe and 400 Oe to the MTJ (see **Figure 2.10(a)**) for the 10 ns to give sufficient time for the magnetization (M_y) to switch the MTJ from P to AP. Our findings show that at high frequency i.e., 50 MHz (pulse width of 10 ns), the C_{AP} exceeded C_P as depicted in **Figure 2.10(a)**, and the TMC became negative or approached zero at the parameters specified in **Table 2.1** and **Table 2.2**. Furthermore, the field-assisted STT switching accelerated the magnetization reversal of the MTJ. Following the magnetization reversal, a sinusoidal voltage of 200 mV and a frequency of 30 Hz is applied to the MTJ device after 20 ns. The dynamic response at the low frequency of capacitance and resistance with respect to the biasing voltage is presented in **Figure 2.10(b)**. It is worth noting that the TMC (%) variation was inversely proportional to the TMR (%), *i.e*., an increase in TMC corresponded to a decrease in TMR with respect to the bias voltage. Additionally, in **Figure 2.11(a)** and **2.11(b)**, we observe that, the transient response of capacitance C_P and C_{AP} at 100 Hz and 1 kHz, respectively, under no/zero bias. These show the dependence of the P and AP capacitance of MTJ on the frequency, which was also shown in **Figure 2.8**; however, at 100 Hz, the values of C_P and C_{AP} are of a few fF, *i.e*., approximately 31 fF and 7 fF, respectively. This value further decreases at a higher frequency of 1 kHz (see **Figure 2.11(b)**) in agreement with the trend observed using experimental data. Moreover, **Figures 2.11(c)** and **2.11(d)** depict the behaviour of C_{AP} and C_P when subjected to a sinusoidal bias voltage with peak values of 0 mV, 50 mV, and 100 mV at a frequency of 160 Hz using a transient response.

Finally, a comparative analysis in **Table 2.3** presents the physical effects included in prior literature and in the proposed work to show the advancement achieved.

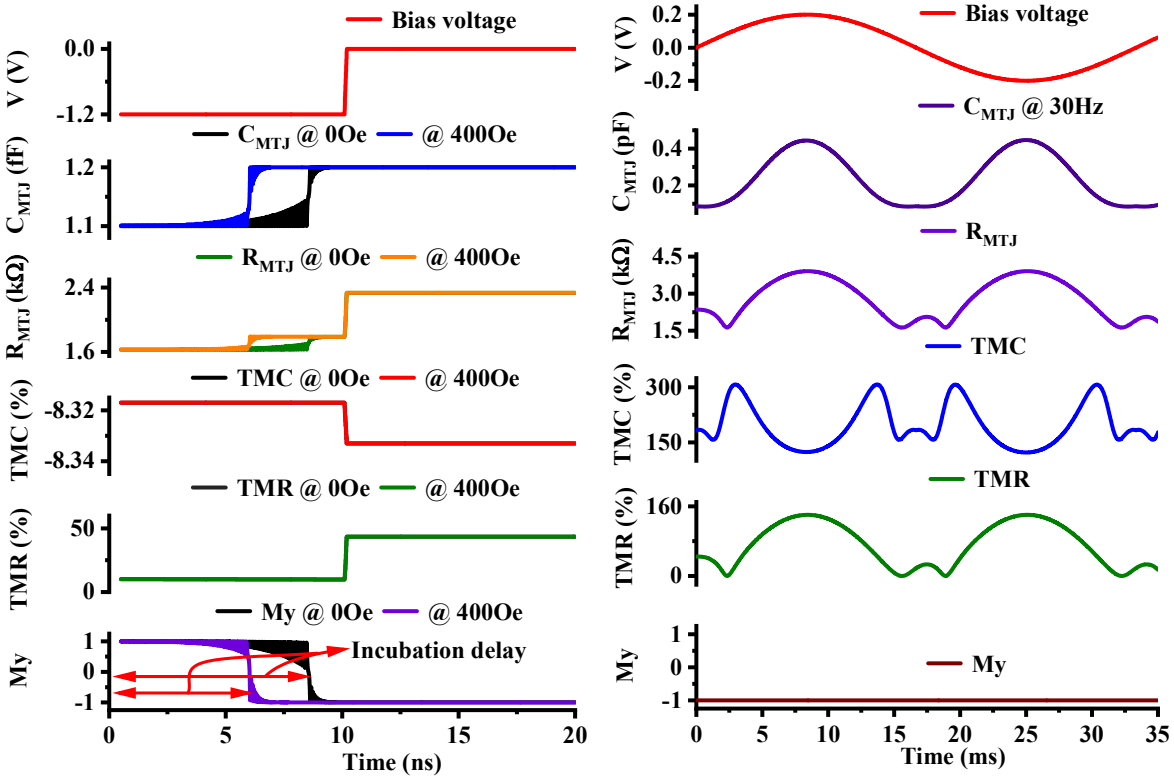

Figure 2.10 (a) Transient analysis at high frequency *i.e.,* 50 MHz (pulse width of 10 ns), to switch the magnetization (M_y) of MTJ from P to AP through only STT (using an external magnetic field of 0 Oe) and field-assisted STT (using an external magnetic field of 400 Oe) switch mechanism, (b) transient analysis at the low-frequency of 30 Hz using low-amplitude (200 mV) of sinusoidal voltage to observe the magnetocapacitance and magnetoresistance.

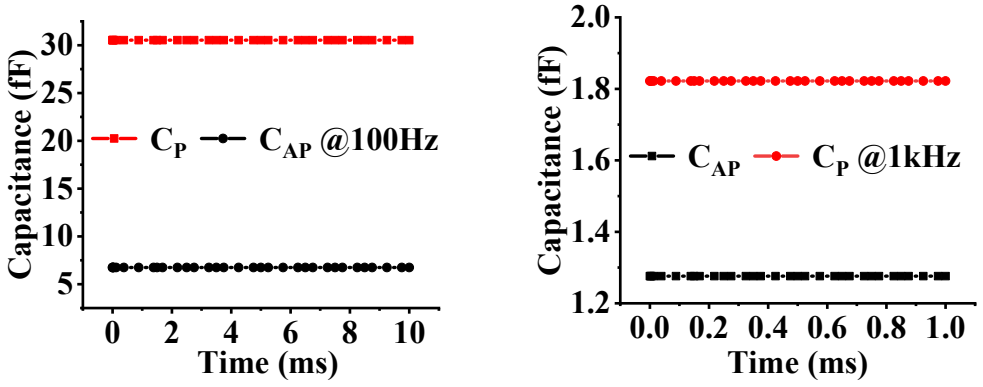

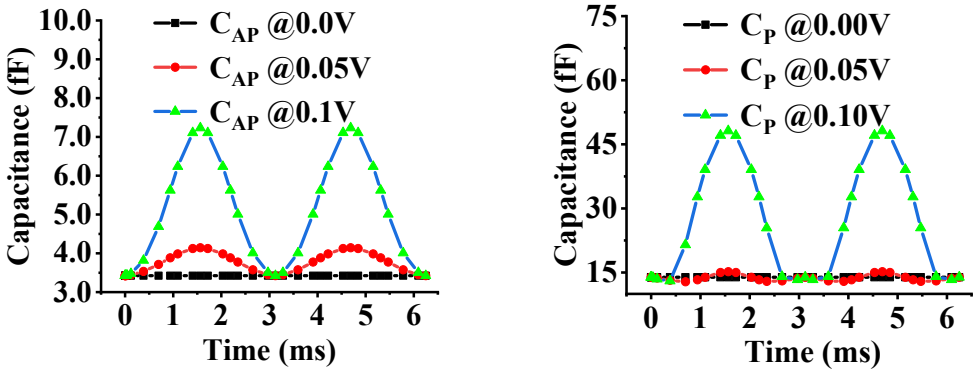

(c) (d)

Figure 2.11 Transient response of C_P and C_{AP} at (a) 100 Hz, (b) 1 kHz, under no bias, and (c) C_{AP} and (d) CP, at the sinusoidal bias voltage with the peak value of 0 mV, 50 mV, and 100 mV at 160 Hz.

Table 2.3 Comparison Between MTJ Compact Models

Model effects/ Parameters	**Zhang** [121]	**Panagopoulos** [95]	**Kazemi** [120]	**De Rose** [177]	**Our model**
Coding Language /Software	Verilog-A /Cadence	SPICE Subckt /HSPICE	Verilog-A /Cadence	Verilog-A /Cadence	SPICE Subckt /HSPICE
MTJ Mag. Anisotropy	PMA	PMA/IMA	PMA/IMA	PMA	PMA/IMA
Thermal Noise Variation	NO	YES	NO	YES	YES
Operating Frequency	High	High	High	High	Low/High
STT Switching	YES	YES	YES	YES	YES
Ext. field-assisted STT	NO	YES	NO	NO	YES
Heat diffusion	NO	YES	YES	YES	YES
Magnetocapacitance effect	NO	NO	NO	NO	YES

2.5 Conclusion

This chapter presented the SPICE-compatible STT-MTJ model, which incorporated both TMC as well as TMR effects. The simulation results validated the accuracy of the proposed compact model that accurately captures magnetocapacitance and TMC effect. The model showed good alignment with experimental data. Hence, this model offers a novel pathway for implementing spintronics applications based on TMC effects, such as non-volatile logic-in-memory circuits, highly sensitive magnetic sensors, designing read-out circuits for sensors, neuromorphic computing, etc.